

## Polyglutamic acid as raw material for drug carriers

H. Guo<sup>a</sup>, L. Fan<sup>a</sup>, L. Ding<sup>a</sup>, H. L. Hou<sup>a</sup>, W. Q. Yang<sup>a</sup>, S. J. Fan<sup>b,\*</sup>

<sup>a</sup>*Department of Scientific Research, Qiqihar Medical University, Qiqihar, 161006, China*

<sup>b</sup>*Research Institute of Medicine & Pharmacy, Qiqihar Medical University, Qiqihar, 161006, China*

$\gamma$ -PGA-PAE nanomaterials were prepared by spontaneous assembly of  $\gamma$ -PGA through condensation reaction, and preparation process of nanomaterials was optimized. HCPT/PGA-PAE nanospheres were prepared by using 10-hydroxycamptothecin as embedding drug, and the nanospheres prepared under the optimal conditions were characterized. The results showed that  $\gamma$ -PGA-PAE nanomaterials were successfully prepared with spherical shape and uniform distribution. HCPT/PGA-PAE nanospheres had high encapsulation rate and drug loading. The optimization of the processing conditions of nanomaterials by response surface method (RSM) is a feasible method to improve the utilization rate of  $\gamma$ -PGA, which provides a theoretical basis for the synthesis of nanomaterials in the future.

(Received July 22, 2022; Accepted December 6, 2022)

*Keywords:* Polyglutamic acid, Nanoparticles, Response surface methodology, HCPT

### 1. Introduction

Nanotechnology is beholding as congregating expertise of the recent times due to its structural constancy overages and its roles concerning every arena of science. Among the many nanoparticulate systems, micelle-like aggregates or nanoparticles formed with amphiphilic block- or graft- copolymers are currently being studied for possible application as protein carriers.

$\gamma$ -Polyglutamic acid ( $\gamma$ -PGA) is an environmentally friendly polymer material with a high molecular weight. It is easily dispersed, non-toxic, harmless, and edible [1]. It is used as a biological flocculant, drug carrier, and food additive in many fields [2-3]. Its use as a drug carrier is enhanced by its biodegradable properties and ability to assemble and disassemble under certain conditions, which enable the loading and release of therapeutic molecules [4-6]. PGA is a linear polymer that is easily hydrolyzed by acids [7]. Its unified molecular weight can be obtained by adjusting the hydrolysis time [8]; however, its low drug loading efficiency (below 30%) limits its use as a nano-drug carrier [9-10]. It is thus important to improve this aspect to enhance its application.

---

\* Corresponding authors: fansongjie@qmu.edu.cn  
<https://doi.org/10.15251/DJNB.2022.174.1399>

Many polymers, such as alginate [11], and short peptides [12], can be easily synthetically modified by the hydrophobic L-phenylalanine ethyl ester (PAE). PAE modifies PGA by ligating to its -COOH side chain [13]. Ideally, the amphiphilic PGA-PAE products self-assemble into micelles with a homogeneous diameter in aqueous solutions [14]. The modified  $\gamma$ -PGA side chains have a hydrophilic carboxyl group and a hydrophobic benzene ring, and thus self-assembles in the water phase to form amphiphilic nanoparticles. These nanoparticles are widely used because of their high drug loading capacity and bioavailability, good stability, and a wide range of drug loading [15-17], among other advantages. The nanoparticles are formed through self-assembly, and thus their particle sizes have some differences. These differences are reflected in their function and application range. As such, factors affecting the particle size should be explored to enhance their application range.

Camptothecin is a natural ingredient isolated from the stem of *Camptotheca acuminata* [18]. It ranks second after paclitaxel as a natural strong anti-cancer compound [19-20]. 10-Hydroxycamptothecin (HCPT) is a water-insoluble drug derived from Camptothecin [21-22]. Injections that are soluble in water after alkalization are the primary HCPT preparations used in clinical applications. This process leads to unstable preparations, which subsequently cause a decrease in anti-cancer activity and the short half-life of HCPT *in vivo* [23], thus significantly limiting the clinical application of HCPT [24]. Numerous scholars have explored transforming its new dosage form to improve its water solubility and anti-tumor effects and reduce its adverse reactions [25-27].

This study used self-synthesized PGA-PAE under an optimal process as the carrier and the hydrophobic core formed by  $\gamma$ -PGA and L-PAE condensation as a micro-drug library to improve the stability and availability of HCPT. The drug was encapsulated because of its poor solubility to protect the inner core from phagocytosis by the liver phagocytes. This modification caused a slow release of the drug *in vivo* [28], thus prolonging its half-life. The nano drug-loaded particle reduced the toxicity of the HCPT compound and enhanced its curative effect.

## **2. Experimental**

### **2.1. Materials used**

$\gamma$ -PGA was purchased from Wako Pure Chemical Industries Company. L-phenylalanine ethyl ester (L-PAE) and N-(3-Dimethylaminopropyl)-N-ethylcarbodiimide hydrochloride (EDC) were sourced from Aladdin Reagent Company. 10-hydroxycamptothecin (HCPT) and N,N-dimethylformamide (DMF) were obtained from Dalian Meilun Biotechnology Company and Tianjin Komiou Chemical Reagent Company, respectively.

### **2.2. Preparation of small molecule $\gamma$ -PGA**

The macromolecular  $\gamma$ -PGA was degraded by high-temperature acid hydrolysis. The  $\gamma$ -PGA (0.5 g) was placed in a beaker, followed by the addition of ultrapure water (30.0 mL) and 1 mol/L NaOH solution dropwise until the  $\gamma$ -PGA was completely dissolved. HCl (1 mol/L) was then slowly added to the  $\gamma$ -PGA solution, and the pH adjusted to 2.0. The PGA was subsequently hydrolyzed by heating the solution in a water bath set at 98 °C for 30 min, 45 min, 60 min, 75 min, and 90 min, respectively. The solution was then quickly placed on crushed ice to cool, and its pH

adjusted to 7.0. The solution was then centrifuged in an ultrafiltration centrifuge tube, then freeze-drying to obtain a small molecule  $\gamma$ -PGA.

### 2.3. Polyacrylamide gel electrophoresis (SDS-PAGE)

All samples were resolved using 12% separation gel (resolving gel) and 5% stacking gel [29]. After the conjugation experiments, all samples were mixed with SDS sample buffer (1:1 ratio), heated for 3 min at 100 °C, and then cooled down to room temperature. After that, 5  $\mu$ L of protein marker and 20  $\mu$ L of each sample were loaded into the wells. The separation gel was subjected to a pre-electrophoresis voltage of 75 V, which was then increased and maintained at 115 V. The electrophoresis was stopped when the bromophenol blue indicator had 1-2 cm away from the front. The gel was then cut appropriately, fixed in a fixing solution [50% methyl alcohol (v/v) and 10% glacial acetic acid (v/v)] for 1 h, and then immersed in methylene blue staining solution on a shaker. Shaking was slowly done at room temperature for 2 h to stain the gel, followed by gel decolorization and capturing the gel imaging analysis system.

### 2.4. Preparation of $\gamma$ -PGA-PAE nanomaterials

The catalyst EDC and L-PAE were added to the small molecule  $\gamma$ -PGA solution, and the reaction shook for different times. The reaction mixture was subsequently centrifuged to remove the supernatant, and the pellet was washed thrice using ultrapure water to remove the unreacted substances. The pellet, which was the  $\gamma$ -PGA-PAE nanomaterials, was then freeze-dried and stored.

### 2.5. Single-factor test

The single factor test was employed to explore the process conditions for preparing the  $\gamma$ -PGA-PAE nanomaterials. Table 1 shows the test design, including the influencing factors, units, and test levels.

Table 1. The single factor test design.

Variable	Unit	Level				
		1	2	3	4	5
$\gamma$ -PGA quality	g	0.025	0.05	0.1	0.2	0.3
EDC quality	g	0.01	0.03	0.07	0.10	0.15
L-PAE quality	g	0.005	0.01	0.02	0.05	0.10
Temperature	°C	20	30	37	45	50
Time	h	12	24	32	48	60
Rotational speed	r/min	0	70	140	200	250

### 2.6. Plackett-Burman experimental design

The test was designed using the Design-Expert 8.0 software.  $\gamma$ -PGA quality, EDC quality, L-PAE quality, temperature, rotational speed, and time were selected based on the single-factor test results as the evaluation factors during the nanoparticles preparation process.

The particle size Y was used as the response value, with each factor expressed as a high value (+1) and a low value (-1). Table 2 outlines the design factors and levels of the PB test.

Table 2. Levels and experimental factors of Plackett-Burman design.

Variable code	Variable	Unit	Level	
			Low value (-1)	High value (+1)
A	$\gamma$ -PGA quality	g	0.2	0.25
B	EDC quality	g	0.03	0.04
C	L-PAE quality	g	0.05	0.0625
D	Temperature	°C	37	45
E	Rotational speed	r/min	140	200
F	Time	h	24	32

### 2.7. Central Composite Design test

The test was designed using the Design-Expert 8.0 software. Three factors:  $\gamma$ -PGA quality, L-PAE quality, and rotational speed, that significantly affected the nanoparticles preparation process were selected based on the PB test results as the independent variables. The particle size Y of the nanoparticles was used as the response value. Table 3 outlines the design factors and levels of the CCD test.

Table 3. Factors and levels of central composite design.

Variable code	Components	Unit	Level				
			-1.682	-1	0	1	1.682
A	$\gamma$ -PGA quality	g	0.1659	0.2	0.25	0.3	0.3341
B	L-PAE quality	g	0.041	0.05	0.0625	0.08	0.092
C	Rotational speed	r/min	99.08	140	200	250	284.1

### 2.8. Preparation of HCPT/PGA-PAE nanospheres

The HCPT/PGA-PAE nanospheres were prepared by a precipitation and dialysis method. The  $\gamma$ -PGA-PAE nanomaterials (20.0 mg) and HCPT (5.0 mg) were dissolved in 10 mL of DMF solution, transferred to a dialysis bag, and dialyzed for 24 h. The nano-microsphere solution in the dialysis bag was subsequently filtered through a 0.45  $\mu$ m filter, freeze-dried, and stored at -4 °C.

### 2.9. Morphology

$\gamma$ -PGA-PAE nanomaterials and HCPT/PGA-PAE nanospheres were first diluted to 1 g/L, followed by dropping 10  $\mu$ L of the diluted sample on a plasma-cleaned copper mesh. It was left to dry for 10 min, after which the excess sample was sucked, followed by staining the copper mesh with 10  $\mu$ L of phosphotungstic acid for 1 min. The excess dye solution was let to air-dry naturally, followed by observation of the staining shape using a transmission electron microscope.

### 2.10. Determination of size distribution and Zeta potential

$\gamma$ -PGA-PAE nanomaterials and HCPT/PGA-PAE nanospheres were dispersed in ultrapure water, and their particle size distribution, particle dispersion index (PDI) and Zeta potential were analyzed using a nanoparticle size analyzer.

### 2.11. Fourier transform infrared (FT-IR) spectroscopy

$\gamma$ -PGA,  $\gamma$ -PGA-PAE nanomaterials, HCPT and HCPT/PGA-PAE nanospheres were freeze-dried, dried and ground to form a powder of the specified size, measured by KBr wafer pressing and then by transmission by infrared spectrometer at room temperature, scanning in a wavenumber range of 400-4000  $\text{cm}^{-1}$ .

### 2.12. Drug loading efficiency (DLE) and drug loading content (DLC)

Varying concentrations of DMF-based HCPT solutions were prepared and used to construct a standard curve. HCPT/PGA-PAE nanospheres were dissolved in DMF solution, mixed evenly, and their absorbance was measured at a wavelength of 367 nm using an ultraviolet spectrophotometer. The HCPT content was finally calculated based on the equation of the constructed standard curve. The formulas used to calculate the DLE and DLC percentages were:

$$\text{DLE}(\%) = \frac{\text{loading amount of drug in particles}}{\text{initial feeding amount of drug for loading}} \times 100\% \quad (1)$$

$$\text{DLC}(\%) = \frac{\text{loading amount of drug in particles}}{\text{total weight of particles}} \times 100\% \quad (2)$$

### 2.13. Data analysis

The response surface experimental design was carried out using the Design-Expert v8.0 software. Data were analyzed using the SPSS v23.0 software. The drawings were subsequently done using GraphPad Prism v8.0.2.

## 3. Results and discussion

### 3.1. Preparation of small molecule $\gamma$ -PGA

$\gamma$ -PGA is an outstanding candidate among the natural macro-molecule nano-carriers due to its unique feature. Compared to others, the molecular weight of  $\gamma$ -PGA is relatively easy to control by acid hydrolysis [8]. Fig. 1 shows the SDS-PAGE electrophoresis results of the hydrolyzed small molecule  $\gamma$ -PGA. The molecular weight distribution of the small molecule  $\gamma$ -PGA was different with different hydrolysis times. The  $\gamma$ -PGA was hydrolyzed at 98 °C after 90 min to small molecule PGA with the distribution range of 10.5-29 kD (lane 6). This finding agrees with that of Chen et al.'s [13], who found that the small molecule  $\gamma$ -PGA could be obtained by hydrolyzing for 30 min, while our study took 90 min, which may be due to the different sources of the macromolecule  $\gamma$ -PGA, or the different types and concentrations of acids. Follow-up experiments thus used the small molecule  $\gamma$ -PGA after 90 min of hydrolysis as the carrier of nanomaterials.

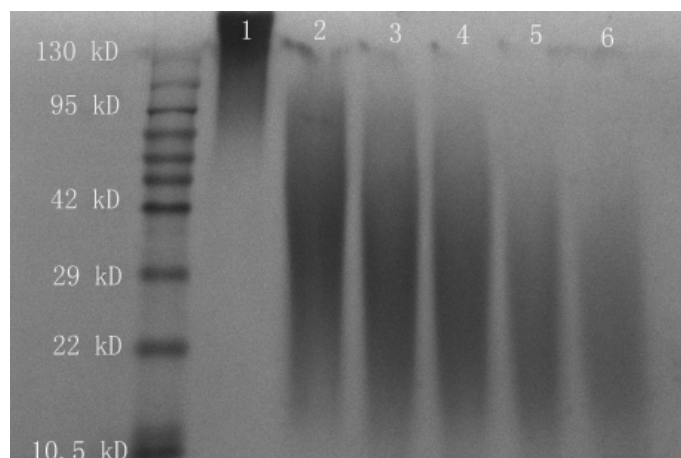


*Fig.1. The SDS-PAGE results of  $\gamma$ -PGA; 1: Unhydrolyzed  $\gamma$ -PGA, 2: Hydrolyzed for 30 min, 3: Hydrolyzed for 45 min, 4: Hydrolyzed for 60 min, 5: Hydrolyzed for 75 min, 6: Hydrolyzed for 90 min.*

### 3.2. Single-factor test results

Amphiphilic graft copolymers composed of  $\gamma$ -PGA as the hydrophilic backbone and L-PAE as the hydrophobic segment were successfully synthesized by grafting L-PAE onto  $\gamma$ -PGA using water-soluble carbodiimide. Due to their amphiphilic properties, the  $\gamma$ -PGA-PAE copolymers were able to form nanoparticles [30].

In this study, with the increase of the main drug concentration, the nanomaterials size showed a change similar to "U", which first decreased and then increased. It may be because when the concentration of the main drug is small, there is a certain chance of combining the nanomaterials, and the nanomaterials size is reduced to a certain extent; when a certain drug concentration is reached, the drugs are in a better state, the combination is more sufficient, and the nanomaterials size reaches the test. As the drug concentration further increases, the viscosity of the liquid increases on the one hand, and on the other hand, the distance between the drugs is too close, which affects the binding effect between the nanomaterials, and the nanomaterials size rebounds. In the process of increasing the rotational speed, the nanomaterials size decreases first, and then increases again. It may be that at a lower rotational speed, the system does not have enough kinetic energy, the collision effect between the nanomaterials is weak, and the nanomaterials size is larger; as the rotational speed increases, the kinetic energy increases, and the nanomaterials size gradually decreases; after reaching a high speed, the nanomaterials size begins to become larger. The possible reason is that the high speed causes some particles to move along the wall due to centrifugal action, which reduces the operation between nanomaterials resulting in the final result. The increase of temperature is beneficial to the formation of nanomaterials, but considering the stability of the drug, the temperature should not be too high, and when the temperature rises to a certain extent, the particle size of the drug also increases.

According to the single-factor test results (Table 4), follow-up tests used 0.2 g of  $\gamma$ -PGA, 0.03 g of EDC, 0.05 g of L-PAE, 37 °C of the temperature, 32 h of the time, and 140 r/min of the rotational speed as the conditions of nanomaterials.

Table 4. Single-factor test results.

Variable	Level	Particle size (nm)	Variable	Level	Particle size (nm)
$\gamma$ -PGA quality (g)	0.025	421.8 $\pm$ 8.4	Temperature ( $^{\circ}$ C)	20	390.6 $\pm$ 6.8
	0.05	376.2 $\pm$ 7.6		30	355.9 $\pm$ 8.5
	0.1	333.2 $\pm$ 8.2		37	187.5 $\pm$ 5.3
	0.2	294.7 $\pm$ 4.6		45	428.0 $\pm$ 9.6
	0.3	566.3 $\pm$ 9.8		50	587.0 $\pm$ 12.1
EDC quality (g)	0.01	376.7 $\pm$ 8.9	Time (h)	12	463.6 $\pm$ 10.8
	0.03	242.1 $\pm$ 4.6		24	308.2 $\pm$ 9.2
	0.07	399.9 $\pm$ 7.9		32	288.5 $\pm$ 4.8
	0.10	494.0 $\pm$ 10.0		48	348.6 $\pm$ 5.7
	0.15	622.5 $\pm$ 9.7		60	563.7 $\pm$ 13.8
L-PAE quality (g)	0.005	416.3 $\pm$ 5.7	Rotational speed (r/min)	0	565.9 $\pm$ 9.6
	0.01	393.3 $\pm$ 5.3		70	363.4 $\pm$ 8.4
	0.02	335.3 $\pm$ 4.9		140	146.5 $\pm$ 5.1
	0.05	295.8 $\pm$ 4.6		200	309.0 $\pm$ 6.5
	0.10	415.1 $\pm$ 8.7		250	584.4 $\pm$ 8.7

### 3.3. Plackett–Burman design

Table 5 outlines the PB experiment design and its results obtained based on the single factor experiment. The  $F$  and  $P$  values of the model were 18.62 and 0.0028 ( $P < 0.01$ ), respectively, suggesting that the model had a great significance (Tab. 6). The model's determination coefficient  $R^2$  was 0.9572, indicating that it could explain 95.72% of the experimental data. In addition, the adjusted determination coefficient  $R^2_{adj}$  was 0.9058 (both connected to 1), with a signal-to-noise ratio of 14.179 ( $> 4$ ), indicating that the model had good predictive power. The significant degree of the influence of each variable on the particle size of the nanomaterials was  $E > A > C > D > F > B$ . The model fitting equation that was obtained after analyzing the data in Table 6 was:  $Y = 216.09 - 28.46A - 3.86B - 20.24C + 6.16D - 44.11E - 4.28F$ .

Table 5. Design and results of Plackett-Burman experiments.

Run	A	B	C	D	E	F	Y Particle size
1	1	1	-1	1	1	-1	151.4
2	-1	-1	-1	1	1	1	246.0
3	1	1	-1	1	-1	-1	277.5
4	1	-1	1	-1	-1	-1	226.6
5	-1	-1	-1	-1	-1	-1	294.7
6	-1	-1	1	1	1	-1	191.5
7	1	-1	-1	-1	1	1	153.1
8	1	1	1	-1	1	1	109.4
9	-1	1	1	1	-1	1	259.3
10	1	-1	1	1	-1	1	207.8
11	-1	1	-1	-1	-1	1	295.3
12	-1	1	1	-1	1	-1	180.5

Table 6. Regression analysis results of Plackett-Burman experiments.

Source	Squares	df	Square	F value	P value
Model	38834.81	6	6472.47	18.62	0.0028*
A	9718.52	1	9718.52	27.96	0.0032*
B	178.64	1	178.64	0.51	0.5055
C	4916.70	1	4916.70	14.15	0.0131*
D	455.10	1	455.10	1.31	0.3043
E	23346.54	1	23346.54	67.18	0.0004*
F	219.31	1	219.31	0.63	0.4630
Residual	1737.64	5	347.53		
Cor total	40572.45	11			

Note: \*P value < 0.05 considered to be statistically significant

### 3.4. Central Composite Design

Table 7 shows the CCD test design levels and the response value results of the nanomaterials size based on the PB test.

Table 7. Design and results of central composite design experiments.

Run	A	B	C	Y Particle size
1	1.682	0	0	122.5
2	1	-1	1	148.4
3	-1	1	1	191.5
4	0	0	0	255.8
5	0	0	1.682	207.3
6	0	0	0	259.3
7	1	-1	-1	116.5
8	0	0	0	268.4
9	0	1.682	0	218.1
10	-1	1	-1	197.8
11	0	-1.682	0	124.0
12	0	0	0	238.3
13	0	0	-1.682	142.7
14	-1	-1	-1	119.6
15	0	0	0	238.0
16	1	1	1	186.6
17	1	1	-1	193.9
18	-1.682	0	0	133.6
19	0	0	0	229.5
20	-1	-1	1	197.0

Table 8. Results of the regression analysis of central composite design experiments.

Source	Squares	df	Square	F value	P value
Model	46675.44	9	5175.05	20.36	<0.0001*
A	458.93	1	458.93	1.81	0.2087
B	8794.23	1	8794.23	34.60	0.0002*
C	3057.54	1	3057.54	12.03	0.0060*
AB	230.05	1	230.05	0.91	0.3638
AC	270.28	1	270.28	1.06	0.3267
BC	1888.05	1	1888.05	7.43	0.0214*
A <sup>2</sup>	21959.10	1	21959.10	86.41	<0.0001*
B <sup>2</sup>	8185.34	1	8185.34	32.21	0.0002*
C <sup>2</sup>	7254.15	1	7254.15	28.54	0.0003*
Residual	2541.15	10	254.13		
Lack of fit	1400.60	5	280.10	1.23	0.4137
Cor total	49116.79	19			

Note: \*P value < 0.05 considered to be statistically significant

The difference of the regression model was extremely significant (Tab. 8;  $P < 0.0001$ ). The model's determination coefficient  $R^2$  was 0.9483, whereas its adjusted coefficient of determination  $R^2_{adj}$  was 0.9017. Though  $R^2_{adj}$  was close to  $R^2$ , the value had decreased, suggesting that the model had an insignificant signal-to-noise ratio of 12.983 ( $> 4$ ) and thus had a strong predictive ability. There were no significant differences in the model's lack-of-fitting terms ( $P = 0.4137 > 0.05$ ), indicating that it had a good degree of fit. This finding strongly suggested that the CCD experimental design was reliable. The model fitting equation obtained after analyzing the data in Table 8 was:

$$Y = 247.89 - 5.80A + 25.38B + 14.96C + 5.36AB - 5.81AC - 15.36BC - 39.04A^2 - 23.83B^2 - 22.44C^2.$$

Variables B and C, interaction term BC and two interaction terms of each variable ( $A^2$ ,  $B^2$ , and  $C^2$ ) had a significant effect on the particle size of the nanomaterials ( $P < 0.05$ ).

### 3.5. Response surface interaction analysis

Fig. 2 shows the influence of various factors and interactions on the particle size of the nanomaterials. The interaction relationship between the variables in the regression model is evident from the 3D response surface plot. The ellipse indicates that the interaction between the variables has a significant impact, whereas the circle indicates no significant impact. There was an elliptical interaction between L-PAE quality and the speed in the contour map, indicating significant interaction ( $P < 0.05$ ).

To usage of conservative ways of optimization of biogenic synthesis of nanomaterials by changing one factor at a time like temperature, time, rotational speed,  $\gamma$ -PGA quality, L-PAE quality and EDC quality by keeping other factors constant is difficult, dull, cost-inefficient, long, and likewise incapable to govern reciprocated interactive properties of diverse factors.

RSM method uses mathematical laws and statistics to analyze problems involving many independent variables. RSM aims to achieve the best performance by finding the best values for the variables. The regression model also provides a relationship between the variables and process response, which can be used to predict system response when process parameters change. When plotted as a response against any two process parameters, the regression model represents the surface geometrically. These plots illustrate visually the relationship between response and process parameters. Then, from these contour figures, the optimal values for the parameters affecting the system performance can be visually reported [31]. Multivariate practices are available for experimental designs, which are Box-Behnken Design (BBD), Central Composite Design (CCD), and Doehlert Matrix (DM). In terms of efficiency of design, CCD is more efficient as compared to BBD and DM [32]. A response surface methodology was applied by Ruby Gupta [33] to obtain ferrite nanoparticles.

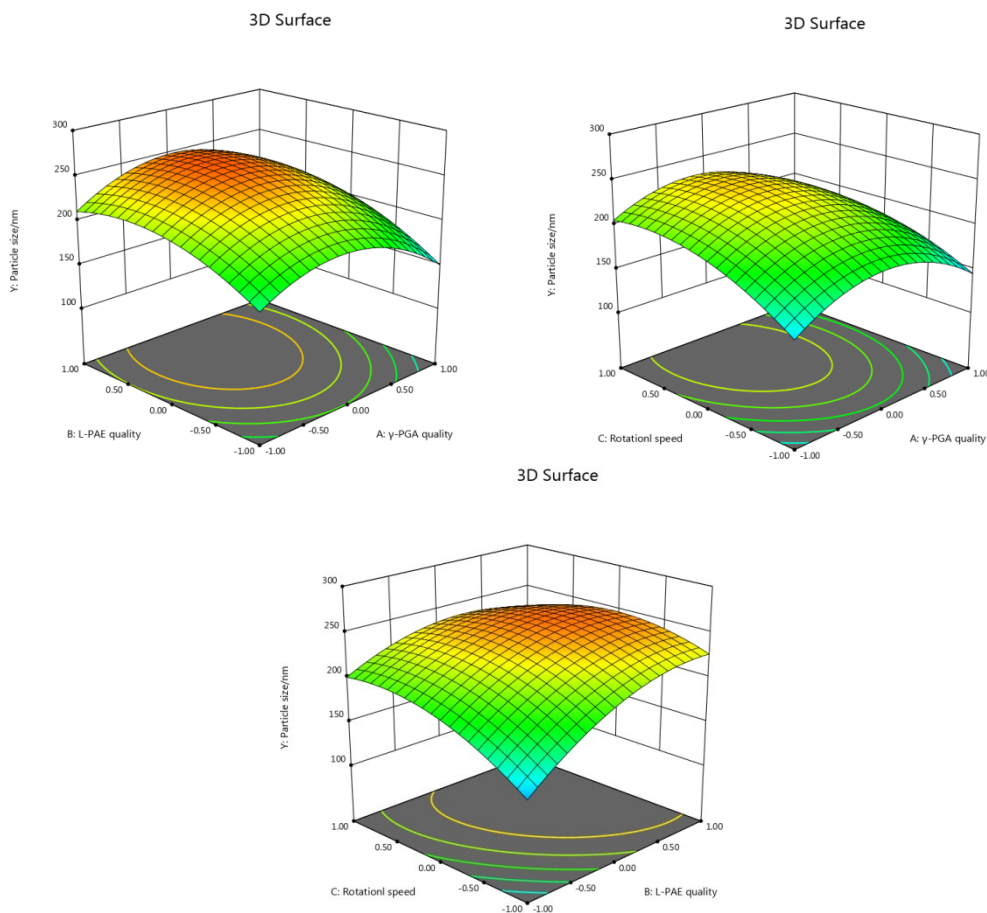


Fig. 2. The influence of the interaction of various factors on the particle size of nanomaterials.

The optimal particle size of nanomaterials in the CCD experiment could be predicted using 0.2 g of  $\gamma$ -PGA, 0.08 g of L-PAE, a rotational speed of 140 r/min, and a nanomaterial size of 182.78 nm. Six factors causing particle size changes during the synthesis of nanomaterials were selected. The optimal process conditions for determining the particle sizes of the nanomaterials were obtained through single factor tests and response surface test optimizations. The particle size of the nanomaterials obtained herein was consistent with those of Chen [13].

### 3.6. Size distribution and Zeta potential

Encapsulation is a process used to protect bioactive compounds from degradation, increase their bioactivity, and modify their physical properties. Recent advances in biopolymer delivery systems have been based on encapsulating bioactive molecules within nanomaterials, which have the advantage of small size [34].

The particle size was in the scope of nanomedicine, therefore, their size is an important factor affecting treatment efficiency [35]. Currently, nanospheres of less than 400 nm are used in clinical applications. This scale range is more suitable for particles required for blood circulation [36-37]. In addition, the PDI measures the molecular weight distribution of polymers, and a smaller PDI means a uniform distribution. In general, a value lower than 0.3 was considered as good polymer dispersion [38]. The results of the particle size for of  $\gamma$ -PGA-PAE nanomaterials and

HCPT/PGA-PAE nanospheres are shown in Fig. 3. Based on Fig. 3, the average particle size of  $\gamma$ -PGA-PAE nanomaterials were  $146.5\pm 2.3$  nm (Fig. 3A), with a PDI of  $0.243\pm 0.013$ , whereas the HCPT/PGA-PAE nanospheres were normally distributed with an average size of  $124.0\pm 5.8$  nm (Fig. 3B) and a PDI of  $0.282\pm 0.021$ . These findings indicated that the HCPT/PGA-PAE nanospheres had a better dispersibility and stability than the  $\gamma$ -PGA-PAE nanomaterials. Moreover, they had a relatively uniform size distribution. The PDI values in all experiments was around 0.2, remaining below 0.3, which is regarded as the value necessary for satisfying particle distribution and uniformity.

The zeta potential can be regarded as an indicator of the stability of a dispersion system. A higher zeta potential makes particles repel one another, resulting in a more stable dispersion [39]. Generally, the border between a stable and an unstable system in aqueous phase is regarded as +30 or -30 mV [40]. The Zeta potential of the HCPT/PGA-PAE nanospheres was -27.58 mV, whereas that of the  $\gamma$ -PGA-PAE nanomaterials was -15.48 mV. The absolute value of the Zeta potential increased, indicating that the HCPT/PGA-PAE nanospheres had excellent stability. It is precisely because the zeta potential of the HCPT/PGA-PAE nanospheres was high enough to support that these nanospheres could not aggregate much in aqueous state in general and in physiologically relevant media in particular [41]. This negative charge of  $\gamma$ -PGA-PAE nanomaterials surfaces is due to the carboxyl groups of  $\gamma$ -PGA. The structure of the nanomaterials is a core-shell type with a L-PAE core and an outer  $\gamma$ -PGA shell. However, as compared to amphiphilic block copolymers, these  $\gamma$ -PGA-PAE nanomaterials possess a very short hydrophobic domain. As a result, it is suggested that the core of nanomaterials consists not only of L-PAE, but also of the  $\gamma$ -PGA that makes up the main chain. Hydrophilic domains are either exposed to aqueous solvents or to low levels of hydrophilic domains within nanomaterials. This finding agrees with that of Akagi et al.'s [42], who synthesized 200 nm-sized nanoparticles by a precipitation method consisting of  $\gamma$ -PGA as the hydrophilic backbone and L-PAE as the hydrophobic side chain. Shen et al. [43] reported the average particle size of nanoparticle fabricated with  $\gamma$ -PGA and L-PAE was  $79\pm 18$  nm, with a PDI of 0.18.

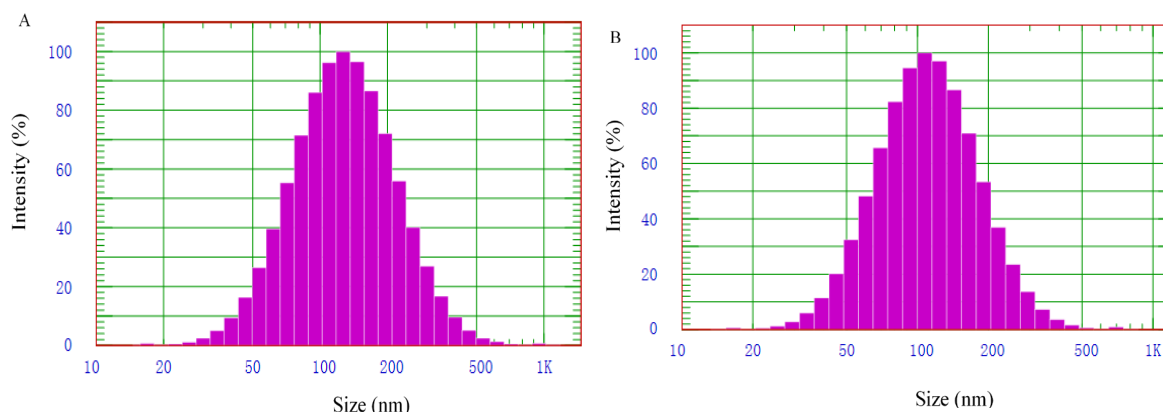


Fig. 3. The size distribution of  $\gamma$ -PGA-PAE nanomaterials and HCPT/PGA-PAE nanospheres.

A:  $\gamma$ -PGA-PAE nanomaterials, B: HCPT/PGA-PAE nanospheres.

### 3.7. Morphology

Fig. 4 showed the transmission electron microscopy results of  $\gamma$ -PGA-PAE nanomaterials and HCPT/PGA-PAE nanospheres. The  $\gamma$ -PGA-PAE nanomaterials had uniform size, a core structure, were spherical or elliptical, uniformly dispersed, and a central hydrophobic core (Fig. 4A and B). They were surrounded by a black-gray hydrophilic shell and had a diameter of about 100 nm, which was in accordance with the result of a nanoparticle size analyzer.

Fig. 4C and D showed the uniformly dispersed HCPT/PGA-PAE nanospheres with a diameter of about 80 nm. The HCPT/PGA-PAE nanospheres were a typical spherical structure in TEM images, and there was no aggregation or adhesion between each other. The HCPT/PGA-PAE nanospheres were significantly smaller than the  $\gamma$ -PGA-PAE nanomaterials, which consistent with the variation of the particle size, further confirmed the particle size measurement. However, the particles size obtained from the TEM image was different from a nanoparticle size analyzer data. This difference can be attributed to change in particle size between the dried and hydrated states. In the case of TEM, the TEM image represents the particle size in a dried sample, whereas a nanoparticle size analyzer method entails measurement of the particle size in a hydrated state [42].

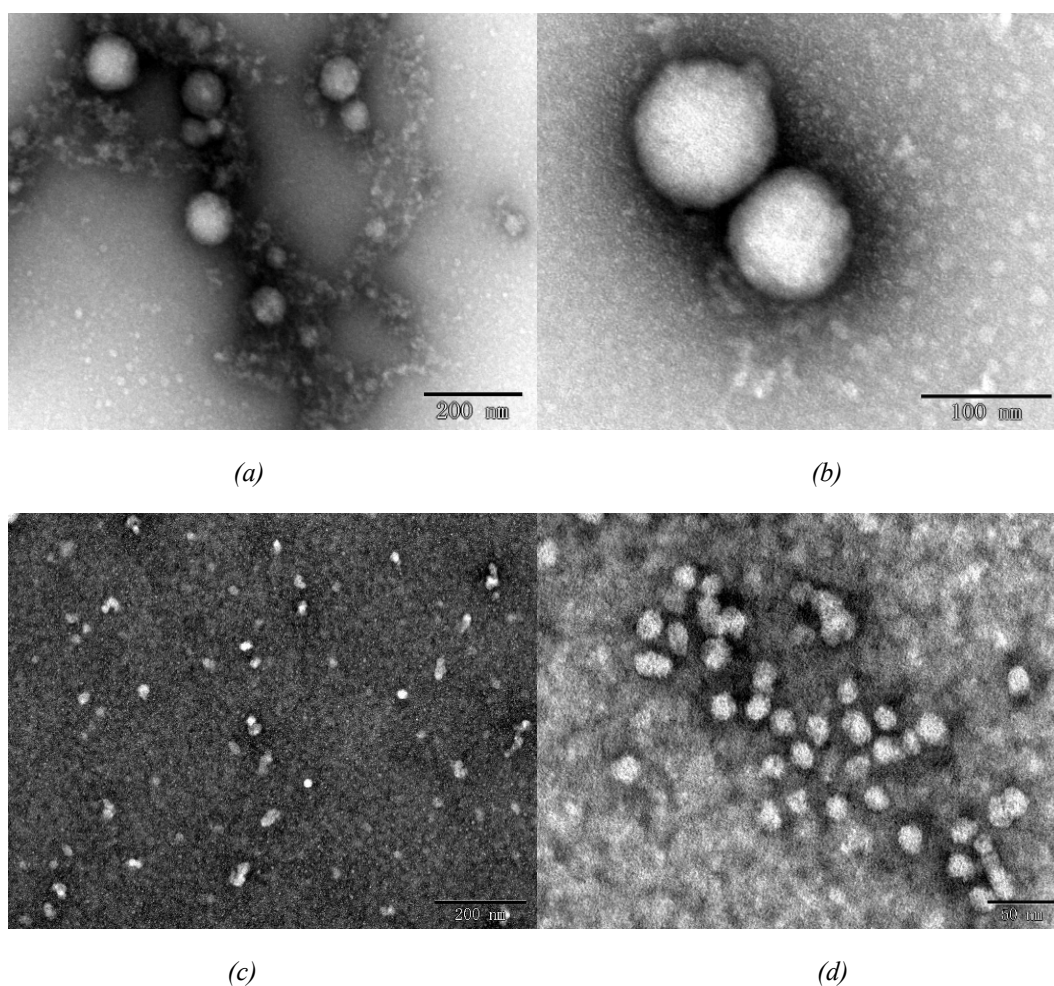


Fig. 4. TEM images of  $\gamma$ -PGA-PAE nanomaterials and HCPT/PGA-PAE nanospheres. A and B:  $\gamma$ -PGA-PAE nanomaterials; C and D: HCPT/PGA-PAE nanospheres.

### 3.8. FT-IR spectrum scanning

Fig. 5 shows FT-IR spectra of  $\gamma$ -PGA,  $\gamma$ -PGA-PAE nanomaterials, HCPT and HCPT/PGA-PAE nanospheres. The  $\gamma$ -PGA-PAE nanomaterials is made by the amidation reaction of the -COOH on the  $\gamma$ -PGA backbone with the -NH<sub>2</sub> on the L-PAE. In the FTIR spectrum of  $\gamma$ -PGA, the peak of 3280 cm<sup>-1</sup> corresponds to the -OH bond, the peaks of 2920 cm<sup>-1</sup> correspond to the -NH bond, and the peaks of 1530 cm<sup>-1</sup> correspond to C-N bond. After L-PAE modification, a new peak appeared at 1640 cm<sup>-1</sup>, a characteristic peak of -C=O on the amide bond, indicating that the  $\gamma$ -PGA-PAE nanomaterials was successfully prepared. For HCPT, the strong peak at 1745 cm<sup>-1</sup> arises from the -C=O stretching vibration of the terminal lactone ring, the characteristic band at 1655 cm<sup>-1</sup> is assigned to the stretching vibration of acylamino group, and the peaks at 1582 and 1501 cm<sup>-1</sup> are corresponding to the skeletal vibrations of aromatic ring [44]. Compared to  $\gamma$ -PGA-PAE nanomaterials, the peak at approximately 1658 cm<sup>-1</sup> for -C=O on the amide bond became sharper and shifted to lower wave numbers in HCPT/PGA-PAE nanospheres. In addition, the peak at 1743 cm<sup>-1</sup> corresponding to the lactone ring of HCPT remains in the spectrum, indicating that the HCPT moieties as their lactone form exist in the HCPT/PGA-PAE nanospheres. The results were in agreement with the findings regarding the loading of HCPT into nanospheres by other previous studies [45-47].

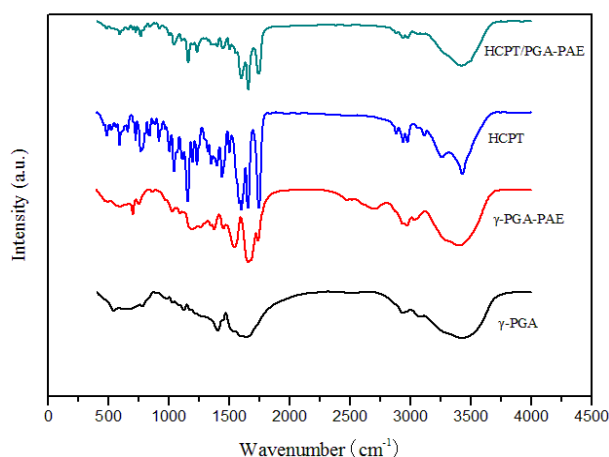


Fig. 5. FT-IR spectrum scanning.

### 3.9. DLE and DLC of the HCPT/PGA-PAE nanospheres

Table 9 highlights the yield, encapsulation efficiency, DLE and DLC of the HCPT/PGA-PAE nanospheres obtained during the preparation process. Their encapsulation rate on the drug was 47.20%, with a drug loading content of 15.73%. The membrane dialysis method used in this study for self-assembling HCPT/PGA-PAE nanospheres does not require dispersants and chemical stabilizers. The micelle preparation efficiency is high, and organic solvents such as DMF can be removed during dialysis [48]. The drug loading content in this study was significantly higher than that of the HCPT sustained-release nanospheres prepared by Yao [49], (1.22%) using the adsorption-coating method.

Table 9. The yield, entrapment efficiency, DLE and DLC of the product.

	The yield (mg)	encapsulation efficiency (%)	DLE (%)	DLC (%)
$\gamma$ -PGA-PAE	119.10	38.42	—	—
HCPT/PGA-PAE	15.01	60.04	47.20	15.73

#### 4. Conclusions

This study successfully formed nanospheres through condensation of hydrophilic  $\gamma$ -PGA and hydrophobic L-PAE in a preparation optimized by changing the influencing factors. The HCPT was subsequently encapsulated with the nanomaterials prepared using the optimal technology to form nanospheres. The encapsulation rate was 47.20%, whereas the drug loading content was 15.73%. Therefore, all of the experiments within the design resulted in acceptable physicochemical properties of HCPT/PGA-PAE nanospheres and can be considered adequate preparation conditions for optimizing  $\gamma$ -PGA-PAE nanomaterials by RSM. This study provides a new and effective way for tumor treatment.

#### Acknowledgements

This work was financially supported by Qiqihar Academy of Medical Sciences Item under Grant No. QMSI2022M-06 and Heilongjiang Provincial Department of education project under Grant No. 2018-KYYWF-0108.

#### References

- [1] Ogunleye A, Bhat A, Irorere VU, Hill D, Williams C, Radecka I, *Microbiology* 161, 1(2015); <https://doi.org/10.1099/mic.0.081448-0>
- [2] Luo Z, Guo Y, Liu J, et al., *Biotechnol Biofuels* 9, 134(2016); <https://doi.org/10.1186/s13068-016-0537-7>
- [3] Kim HC, Kim MH, Park WH, *Int J Biol Macromol* 118, 238(2018); <https://doi.org/10.1016/j.ijbiomac.2018.06.035>
- [4] Kunda NK, Alfagih IM, Dennison SR, et al., *Pharm Res* 32, 1341(2015); <https://doi.org/10.1007/s11095-014-1538-5>
- [5] Mukai H, Saeki T, Aogi K, et al., *Cancer Sci* 107, 1465(2016); <https://doi.org/10.1111/cas.13017>
- [6] Li L, Chen L, Zhang H, Yang Y, Liu X, Chen Y, *Mater Sci Eng C Mater Biol Appl* 61,158(2016).
- [7] Ijadi Bajestani M, Mousavi SM, Mousavi SB, Jafari A, Shojaosadati SA, *Int J BiolMacromol* 113, 142(2018); <https://doi.org/10.1016/j.ijbiomac.2018.02.082>

- [8] Totani K, Kubota T, Kuroda T, et al, *Glycobiology* 13, 315(2003);  
<https://doi.org/10.1093/glycob/cwg032>
- [9] Xiong Y, Jiang W, Shen Y, et al, *Biomaterials* 33, 7182(2012);  
<https://doi.org/10.1016/j.biomaterials.2012.06.071>
- [10] Geng X, Ye H, Feng Z, et al., *J Biomed Mater Res A* 100, 2839(2012);  
<https://doi.org/10.1002/jbm.a.34207>
- [11] Gong X, Branford-White C, Tao L, et al., *Mater Sci Eng C Mater Biol Appl* 58, 478(2016);  
<https://doi.org/10.1016/j.msec.2015.08.059>
- [12] Datta D, Tiwari O, Ganesh KN, *Nanoscale* 10, 3212(2018);  
<https://doi.org/10.1039/C7NR08436F>
- [13] Chen Y, Zhang L, Liu Y, et al., *ACS Appl Mater Interfaces* 10, 25006(2018);  
<https://doi.org/10.1021/acsami.8b04259>
- [14] Zhao P, Zheng M, Yue C, et al., *Biomaterials* 35, 6037(2014);  
<https://doi.org/10.1016/j.biomaterials.2014.04.019>
- [15] Zhang M, Yang J, Yang Q, et al., *Int J Biol Macromol* 112, 1156(2018).
- [16] Ozdemir M, Karapinar B, Yalcin B, et al., *Dalton Trans* 48, 13046(2019);  
<https://doi.org/10.1039/C9DT02687H>
- [17] Pillarisetti S, Maya S, Sathianarayanan S, Jayakumar R, *Colloids Surf B Biointerfaces* 159, 809(2017); <https://doi.org/10.1016/j.colsurfb.2017.08.057>
- [18] Yao L, Zhao X, Li Q, et al., *Int J Pharm* 423, 586(2012);  
<https://doi.org/10.1016/j.ijpharm.2011.11.031>
- [19] Guo M, Rong WT, Hou J, et al., *Nanotechnology* 24, 245101(2013);  
<https://doi.org/10.1088/0957-4484/24/24/245101>
- [20] Zhang ZJ, Shang XF, Yang L, et al., *Front Chem* 7, 922(2019).
- [21] Li R, Wang Y, Yang Q, et al., *AAPS Pharm Sci Tech* 21, 324(2020);  
<https://doi.org/10.1208/s12249-019-1607-5>
- [22] Dong W, Shi J, Yuan T, et al., *Eur J Med Chem* 167, 583(2019);  
<https://doi.org/10.1016/j.ejmech.2019.02.017>
- [23] Cetindere S, Okutan E, Tumay SO, et al., *J Fluoresc* 29, 1143(2019);  
<https://doi.org/10.1007/s10895-019-02424-x>
- [24] Arif M, Raja MA, Zeenat S, et al., *J Biomater Sci Polym Ed* 28, 50(2017);  
<https://doi.org/10.1080/09205063.2016.1242460>
- [25] Zhang ZR, Lu W, Yao Xue Xue Bao 32, 222(1997).
- [26] Chow DS, Gong L, Wolfe MD, et al., *Ann N Y Acad Sci* 922, 164(2000);  
<https://doi.org/10.1111/j.1749-6632.2000.tb07034.x>
- [27] Williams J, Lansdown R, Sweitzer R, et al., *J Control Release* 91, 167(2003);  
[https://doi.org/10.1016/S0168-3659\(03\)00241-4](https://doi.org/10.1016/S0168-3659(03)00241-4)
- [28] Oda M, Koyanagi S, Tsurudome Y, et al., *Mol Pharmacol* 85,715(2014);  
<https://doi.org/10.1124/mol.113.089805>
- [29] Alaneed R, Hauenschild T, Mader K, et al., *J Pharm Sci* 109, 981(2020);  
<https://doi.org/10.1016/j.xphs.2019.10.052>
- [30] Zhang L, Geng X, Zhou J, et al., *J Drug Target* 23, 453(2015);

<https://doi.org/10.3109/1061186X.2014.1003139>

[31] Kong Y, Zou P, Miao L, et al., *Environ Sci Pollut Res Int* 21, 5983(2014);

<https://doi.org/10.1007/s11356-014-2532-5>

[32] Jung JP, Hu D, Domian IJ, et al., *Sci Rep* 5, 18705(2015); <https://doi.org/10.1038/srep18705>

[33] Gupta R, Tomar R, Chakraverty S, et al., *RSC Adv* 11, 16942(2021);

<https://doi.org/10.1039/D1RA02376D>

[34] Desai MP, Labhasetwar V, Amidon GL, et al., *Pharm Res* 13, 1838(1996);

<https://doi.org/10.1023/A:1016085108889>

[35] Arfors KE, Rutili G, Svensjo E, *Acta Physiol Scand Suppl* 463, 93(1979).

[36] Kumar R, Pal P, *Bioresour Technol* 177, 141(2015);

<https://doi.org/10.1016/j.biortech.2014.11.078>

[37] Zhang R, Xu S, Zhu Y, et al., *Biosens Bioelectron* 85, 381(2016).

[38] Gordon S, Teichmann E, Young K, et al., *Eur J Pharm Sci* 41, 360(2010);

<https://doi.org/10.1016/j.ejps.2010.07.004>

[39] Mishra PR, Al Shaal L, Muller RH, et al., *Int J Pharm* 371, 182(2009);

<https://doi.org/10.1016/j.ijpharm.2008.12.030>

[40] Bhattacharjee S, *J Control Release* 235, 337(2016);

<https://doi.org/10.1016/j.jconrel.2016.06.017>

[41] Yang X, Wu S, Wang Y, et al., *Nanoscale Res Lett* 9, 2408(2014);

<https://doi.org/10.1186/1556-276X-9-687>

[42] Akagi T, Higashi M, Kaneko T, et al., *Biomacromolecules* 7, 297(2006);

<https://doi.org/10.1021/bm050657i>

[43] Shen J, Zhao Z, Shang W, et al., *Int J Nanomedicine* 12, 6477(2017);

<https://doi.org/10.2147/IJN.S139602>

[44] Li N, Wang J, Yang X, Li L, *Colloids Surf B Biointerfaces* 83, 237(2011);

<https://doi.org/10.1016/j.colsurfb.2010.11.027>

[45] Guo Y, Wang T, Zhao S, et al., *Mol Pharm* 15,2665(2018);

<https://doi.org/10.1021/acs.molpharmaceut.8b00190>

[46] Wu S, Yang X, Li Y, et al., *Nanoscale Res Lett* 11, 294(2016);

<https://doi.org/10.1186/s11671-016-1491-9>

[47] Kulhari H, Telukutla SR, Pooja D, et al., *Nanomedicine* 12, 1661(2017);

<https://doi.org/10.2217/nnm-2017-0067>

[48] Xu J, Sun Y, Yuan Z, et al., *J Biomed Nanotechnol* 15, 329(2019);

<https://doi.org/10.1166/jbn.2019.2681>

[49] Yao L, Zhao X, Li Q, et al., *Int J Pharm* 423, 586(2012);

<https://doi.org/10.1016/j.ijpharm.2011.11.031>